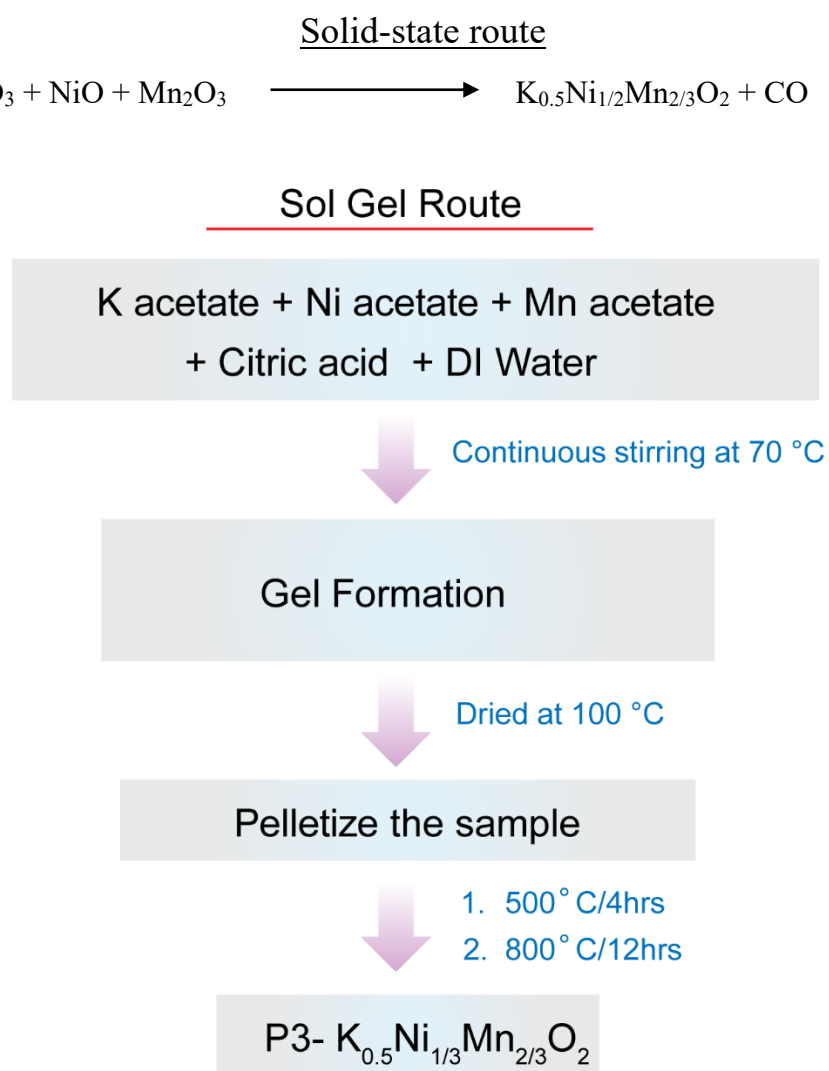


## Supporting Information

### A 3.2 V Binary Layered Oxide Cathode for Potassium-ion Batteries

Pawan Kumar Jha, Shubham Kumar Parate, Krishnakanth Sada, Kazuki Yoshii, Titus Masese, Pavan Nukala, Gopalakrishnan Sai Gautam, Valérie Pralong, Maximilian Fichtner, and Prabeer Barpanda\*



**Figure S1.** (top) Solid-state reaction and (bottom) schematic illustration of sol-gel synthesis for preparation of P3-type  $\text{K}_{0.5}\text{Ni}_{1/3}\text{Mn}_{2/3}\text{O}_2$  (KNM) product.

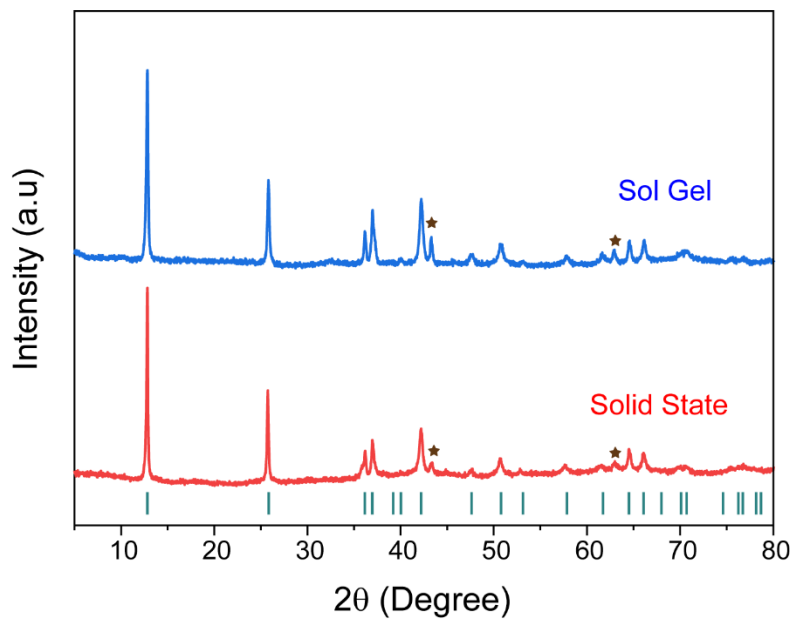
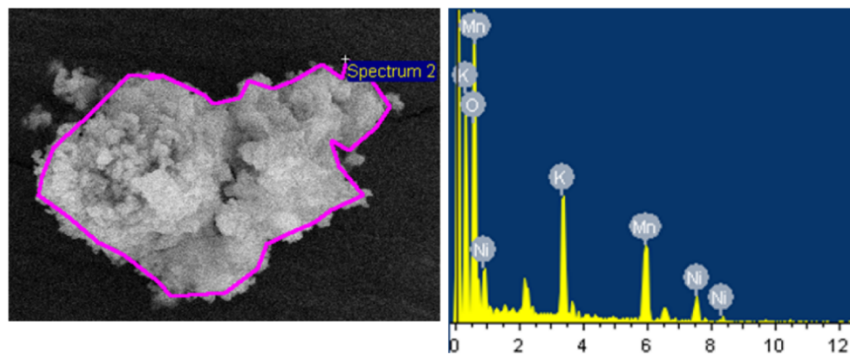


**Figure S2.** Comparative powder X-Ray diffraction patterns of P3-type  $K_{0.5}Ni_{1/3}Mn_{2/3}O_2$  products prepared by solid-state (red) and sol-gel (blue) synthesis routes. Bragg diffraction positions for the Target P3-type phase are shown in green ticks and star symbols represent peak for the minor impurity NiO phase.



Element	Weight%	Atomic%
K	14.47	9.78
O	42.26	69.83
Mn	29.41	14.15
Ni	13.86	6.24

**Figure S3.** Energy-dispersive X-ray spectroscopy (EDS) analysis of P3-type  $K_{0.5}Ni_{1/3}Mn_{2/3}O_2$  particle showing the desired distribution of K, Ni, Mn, and O elements.

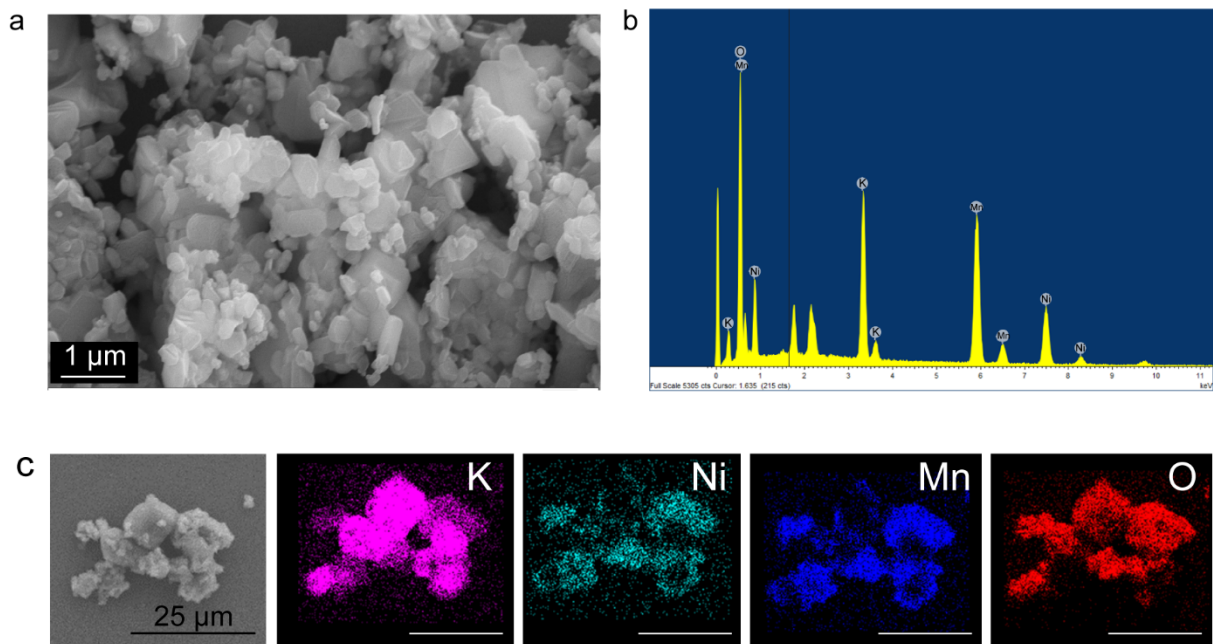


**Figure S4.** (a) SEM micrograph and (b-c) EDS analysis and elemental mapping of P3- $K_{0.5}Ni_{1/3}Mn_{2/3}O_2$  phase synthesize via sol-gel method.

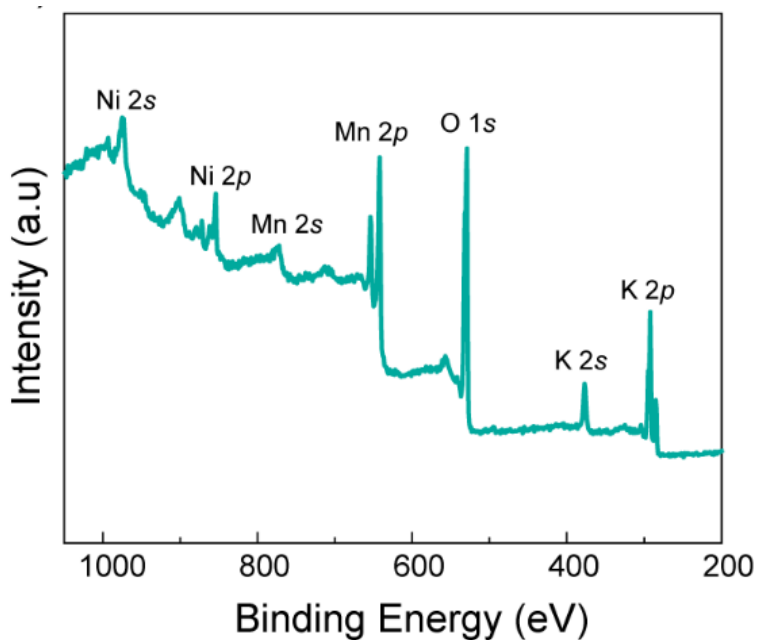


**Figure S5.** XPS survey spectrum of P3-type  $K_{0.5}Ni_{1/3}Mn_{2/3}O_2$  affirming the presence of  $Mn^{4+}$ ,  $Ni^{2+}/Ni^{3+}$  and  $K^+$  in the as-sythesized product.

**Table S1.** The structural and lattice parameters of P3-type  $K_{0.5}Ni_{1/3}Mn_{2/3}O_2$  as derived from Rietveld refinement of XRD pattern ( $\lambda = 1.5405 \text{ \AA}$ ).

<b>Formula (molecular weight)</b>	<b>K<sub>0.5</sub>Ni<sub>1/3</sub>Mn<sub>2/3</sub>O<sub>2</sub> (107.74 g/mol)</b>
<b>Crystal system</b>	Rhombohedral
<b>Space group</b>	<i>R</i> 3 <i>m</i> (#160)
<b>Unit cell parameter (Å)</b>	$a = b = 2.8872 (3)$ $c = 20.6654 (15)$ $\alpha = \beta = 90^\circ, \gamma = 120^\circ, Z = 3$
<b>Unit cell volume (Å<sup>3</sup>)</b>	149.186 (4)
<b>Theoretical density (g cm<sup>-3</sup>)</b>	3.59
<b>Goodness of fit value</b>	$\chi^2 = 8.16\%$

	Site	x	y	z	Occupancy
Ni1	3a	0.000	0.000	0.000	0.66(4)
Mn1	3a	0.000	0.0000	0.0000	0.33(3)
K1	3a	0.000	0.000	0.8360(2)	0.51(5)
O1	3a	0.000	0.000	0.3693(1)	1.0
O2	3a	0.000	0.000	0.6520(5)	1.0

**Table S2.** DFT-calculated and experimentally observed lattice parameters for P3-type K<sub>0.5</sub>Ni<sub>1/3</sub>Mn<sub>2/3</sub>O<sub>2</sub>. PBE and SCAN stand for Perdew-Burke-Ernzerhof and strongly constrained and appropriately normed functionals, respectively. *U* represents the Hubbard U correction. *vdw* signifies the addition of van der Waals corrections.

	<b>a (Å)</b>	<b>b (Å)</b>	<b>c (Å)</b>	<b><math>\alpha</math>(°)</b>	<b><math>\beta</math>(°)</b>	<b><math>\gamma</math>(°)</b>	<b>V (Å<sup>3</sup>)</b>
PBE+ <i>U</i>	2.945	2.937	18.957	89.996	90.844	119.911	142.117
PBE+ <i>U+vdw</i>	2.929	2.917	18.801	90.009	90.689	119.863	139.323
SCAN+ <i>U</i>	2.901	2.888	18.719	90.704	90.462	120.296	135.354
SCAN+ <i>U+vdw</i>	2.875	2.881	18.639	89.359	91.173	119.662	134.142
Experiment	2.891(23)	2.891(23)	20.71(15)	90	90	120	149.95(20)

**Table S3.** DFT (SCAN+ $U$ ) calculated onsite magnetic moments of Mn and Ni along with the corresponding electronic configuration at the potassiated ( $K_{0.5}Ni_{1/3}Mn_{2/3}O_2$ ) and depotassiated ( $Ni_{1/3}Mn_{2/3}O_2$ ) compositions.

Transition Metal	$K_{0.5}Ni_{1/3}Mn_{2/3}O_2$	$Ni_{1/3}Mn_{2/3}O_2$
Mn	$3.03 (4^+) - t_{2g}^3 e_g^0$	$3.03 (4^+) - t_{2g}^3 e_g^0$
Ni	$1.72 (2^+) - t_{2g}^6 e_g^2$ $1.06 (3^+) - t_{2g}^6 e_g^1$	$0.238 (4^+) - t_{2g}^6 e_g^0$

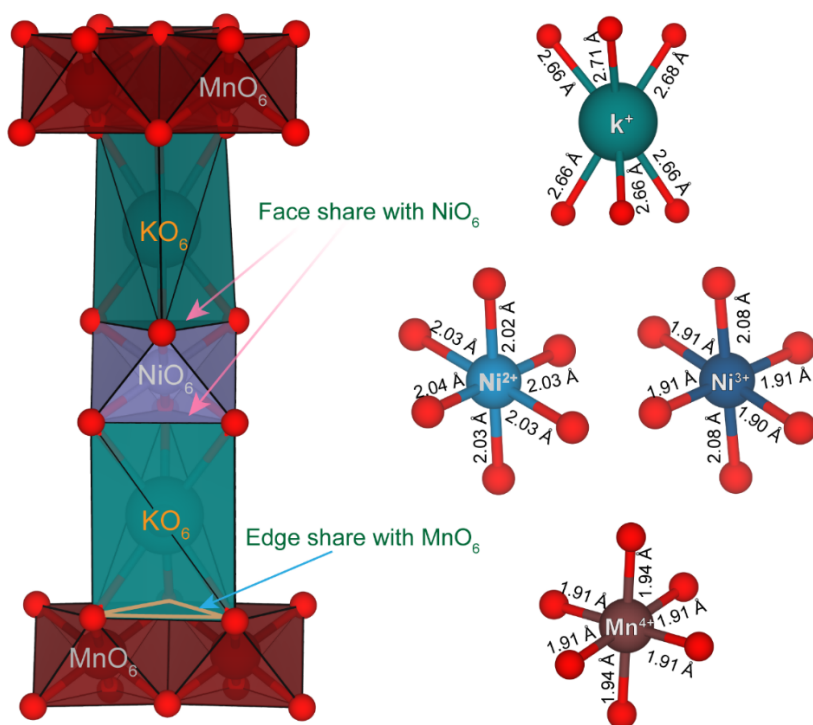


**Figure S6.** A local environment within the DFT (SCAN+ $U$ ) calculated ground state structure of P3-type  $K_{0.5}Ni_{1/3}Mn_{2/3}O_2$ . Right panel displays the bond lengths between K-O, Ni-O and Mn-O.

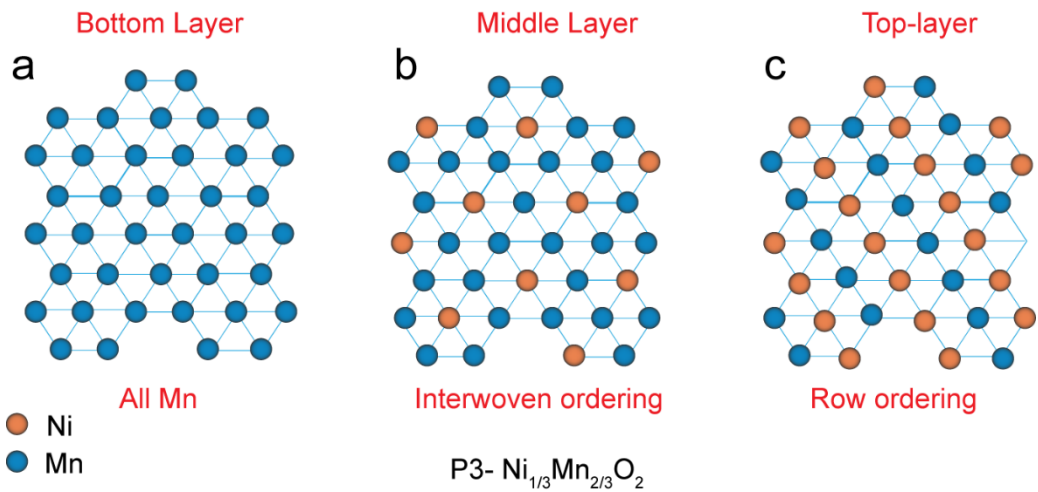


**Figure S7.** DFT (SCAN+ $U$ ) calculated In-plane Ni-Mn ground state ordering at fully depotassiated ( $x = 0$ ) state in  $\text{K}_x\text{Ni}_{1/3}\text{Mn}_{2/3}\text{O}_2$  in the (a) Bottom (Basel), (b) Middle and top M layer, respectively.

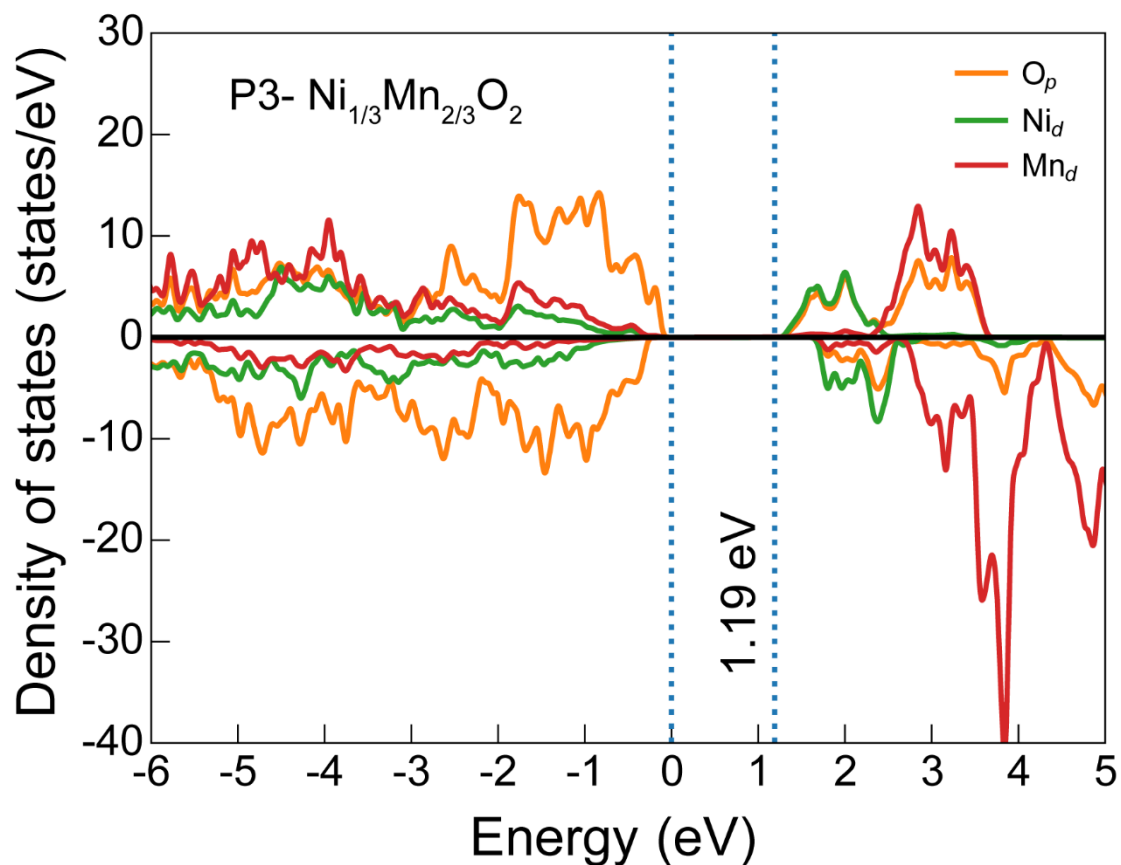


**Figure S8.** DFT (SCAN+ $U$ ) projected density of states for P3- $\text{Ni}_{1/3}\text{Mn}_{2/3}\text{O}_2$ . Orange, green, and red curves represent O  $p$ , Ni  $d$ , and Mn  $d$  states, respectively. Dotted blue lines signify the band edges, with the number indicating the band gap magnitude.

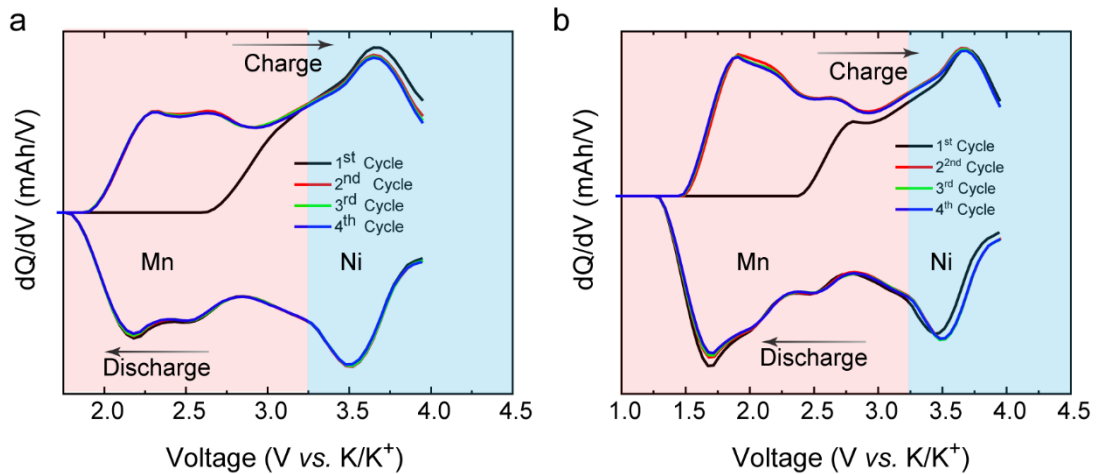


**Figure S9.** Derivative capacity ( $dQ/dV$ ) curve of P3-type  $K_{0.5}Ni_{1/3}Mn_{2/3}O_2$  cathode vs.  $K/K^+$  in (a) 4.2 – 2.0 V (b) 4.2 – 1.5 V potential window.

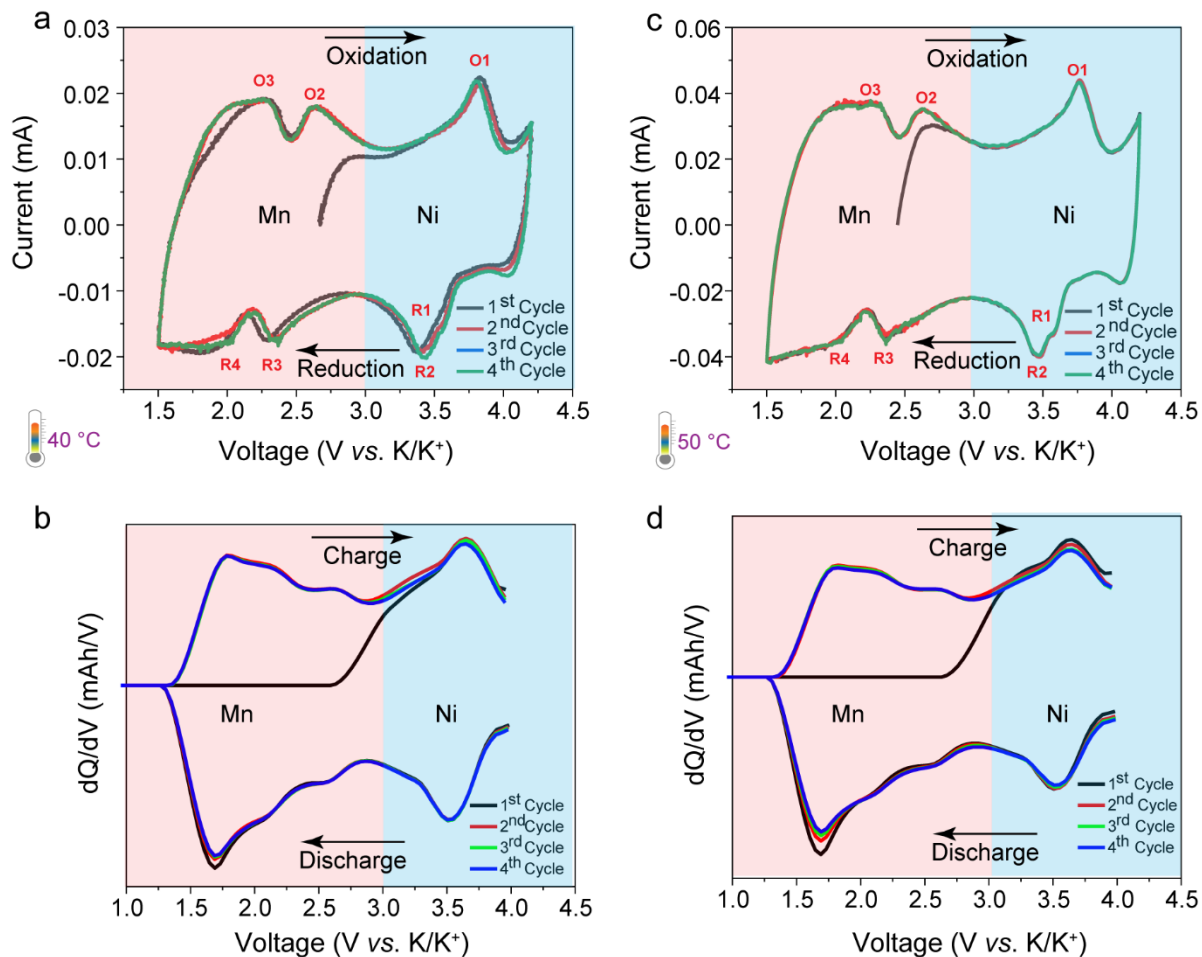


**Figure S10.** Cyclic voltammetry (at the scan rate of  $0.1 \text{ mVs}^{-1}$ ) and derivative capacity ( $dQ/dV$ ) curve of P3-type  $K_{0.5}Ni_{1/3}Mn_{2/3}O_2$  cathode vs.  $K/K^+$  in the potential window of 4.2 – 1.5 V at (a-b) 40°C (c-d) 50°C, respectively.

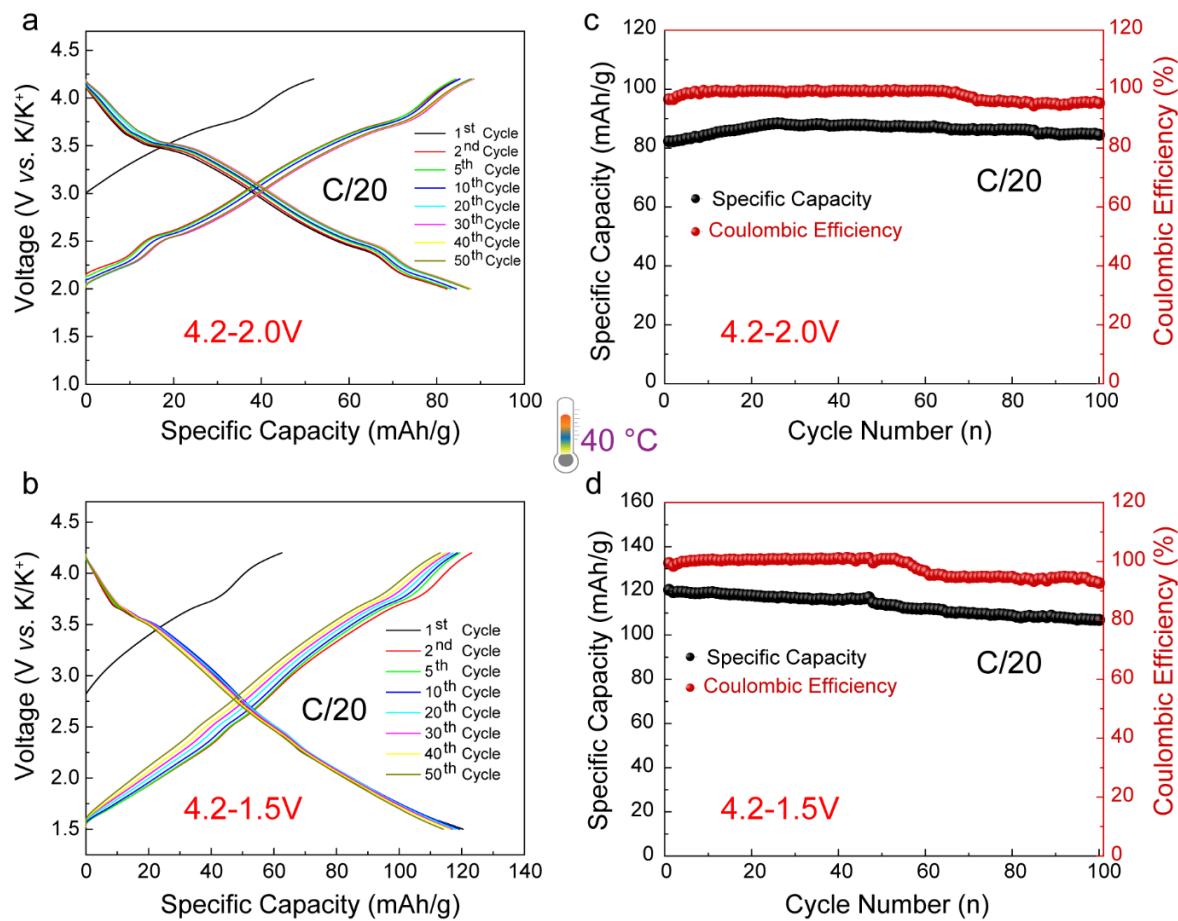


**Figure S11.** Electrochemical performance of P3-type  $K_{0.5}Ni_{1/3}Mn_{2/3}O_2$  cathode at  $40^\circ C$ . a-b) Galvanostatic (dis)charge profiles (vs  $K/K^+$ ) and c-d) Cycling stability curves at a current rate of C/20 in electrochemical potential windows of 4.2 – 2.0 V and 4.2 – 1.5 V.

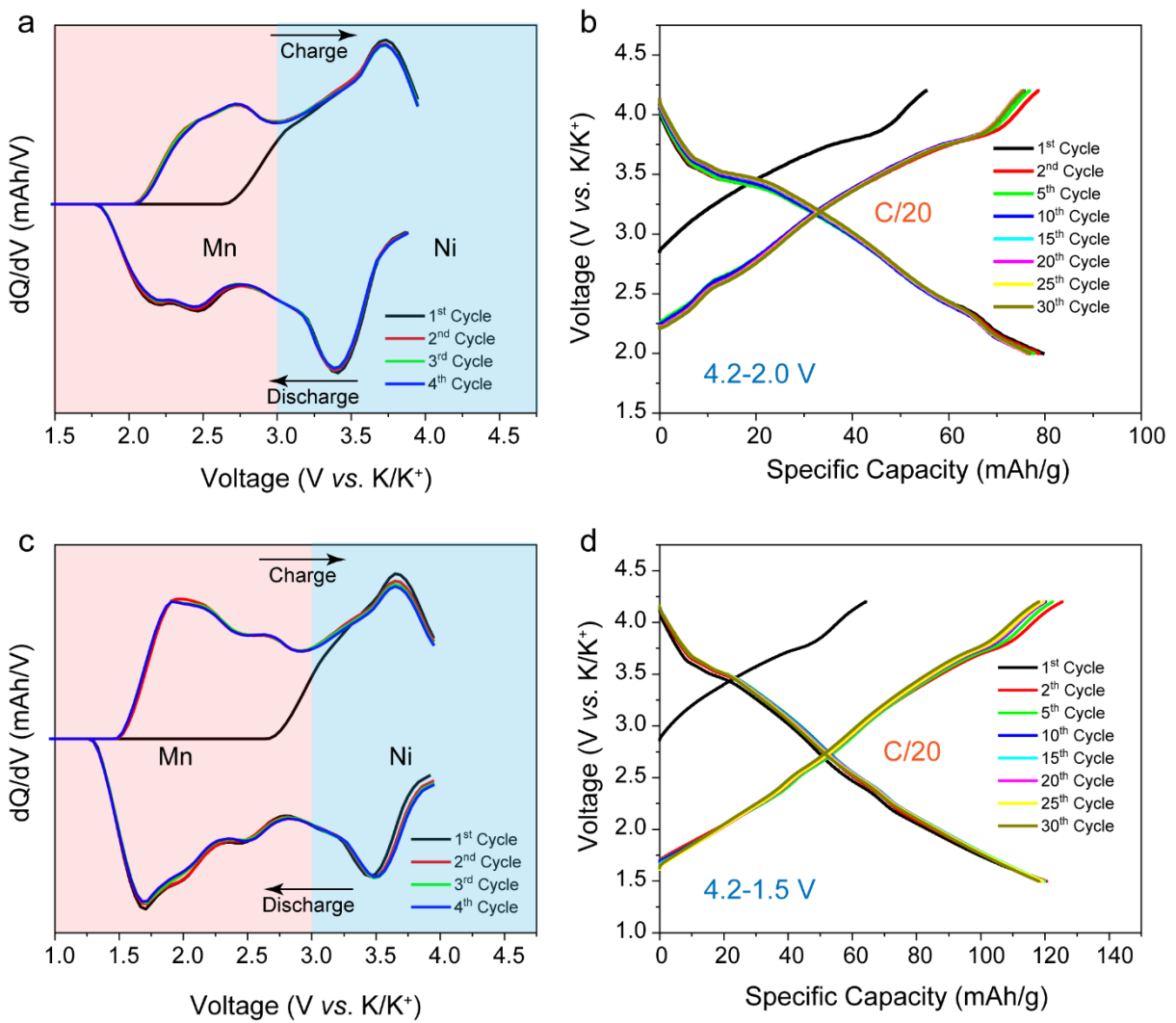


**Figure S12.** Electrochemical performance of P3-K<sub>0.5</sub>Ni<sub>1/3</sub>Mn<sub>2/3</sub>O<sub>2</sub> synthesized via sol-gel route. The Derivative capacity (dQ/dV) curve and Galvanostatic (dis)charge profiles (*vs* K/K<sup>+</sup>) in the (a-b) 4.2-2.0 V (c-d) 4.2-1.5 V voltage window, respectively.

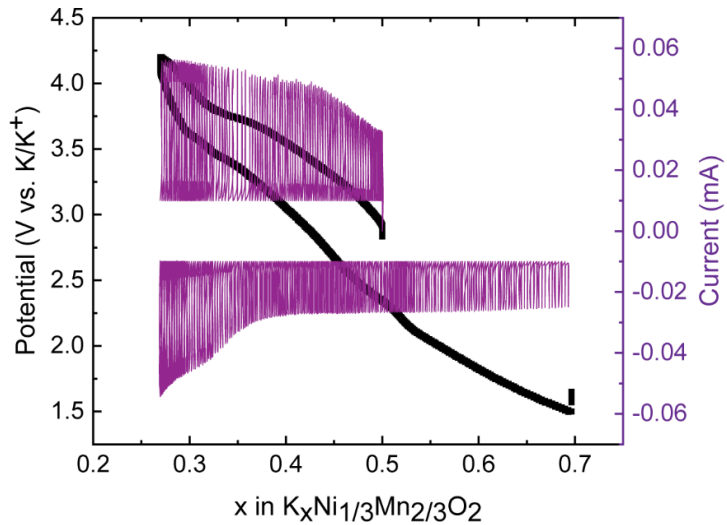


**Figure S13.** Potentiostatic intermittent titration (PITT) curves (vs.  $\text{K}/\text{K}^+$ ) acquired with 10 mV potential steps (purple) and the current decay limited to  $C/50$ , along with the (dis)charge voltage profile (black). The testing employed an active material loading of  $2.2 \text{ mg/cm}^2$  and a current rate of  $5.4 \mu\text{A}$ .

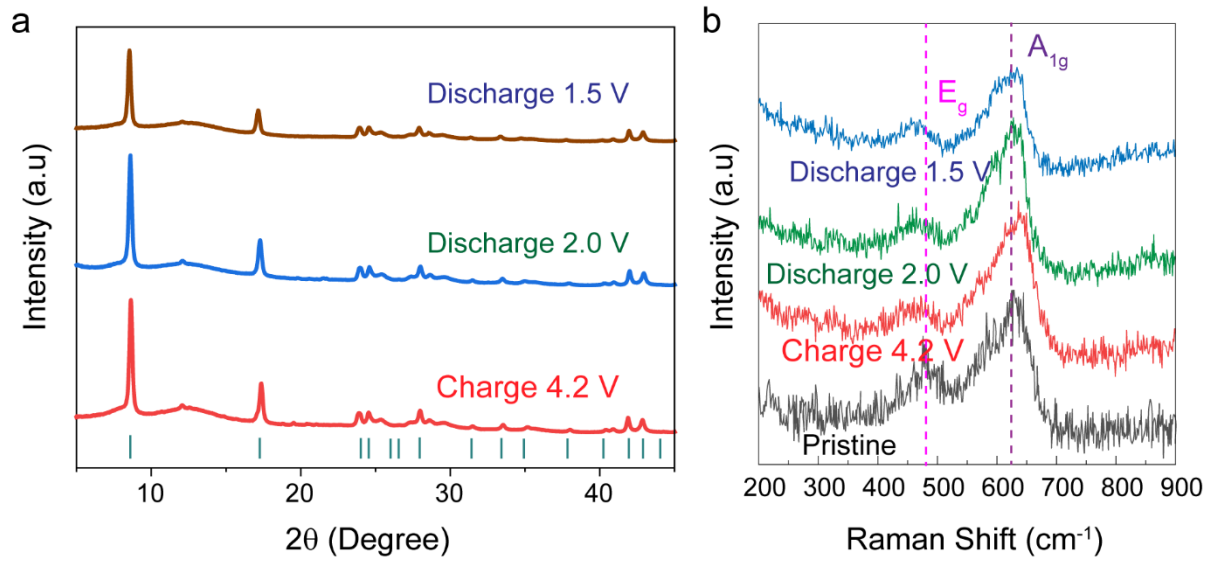


**Figure S14.** Comparative (left) ex-situ synchrotron powder X-Ray diffraction ( $\lambda = 1.033 \text{ \AA}$ ) patterns and (right) Raman spectra of P3-type  $\text{K}_{0.5}\text{Ni}_{1/3}\text{Mn}_{2/3}\text{O}_2$  cathode at different states of (dis)charge. Green ticks represent the Bragg position for the pristine  $\text{K}_{0.5}\text{Ni}_{1/3}\text{Mn}_{2/3}\text{O}_2$  phase.

**Table S4.** Comparative lattice parameters at different states of charge and discharge for P3-type  $K_{0.5}Ni_{1/3}Mn_{2/3}O_2$  cathode.

(Dis)charge State	a (Å)	b(Å)	c(Å)	v(Å <sup>3</sup> )
Ch-4.2V	2.883	2.883	20.736	149.275
Dis-2.0V	2.879	2.879	20.627	148.154
Dis-1.5V	2.886	2.886	20.514	147.999

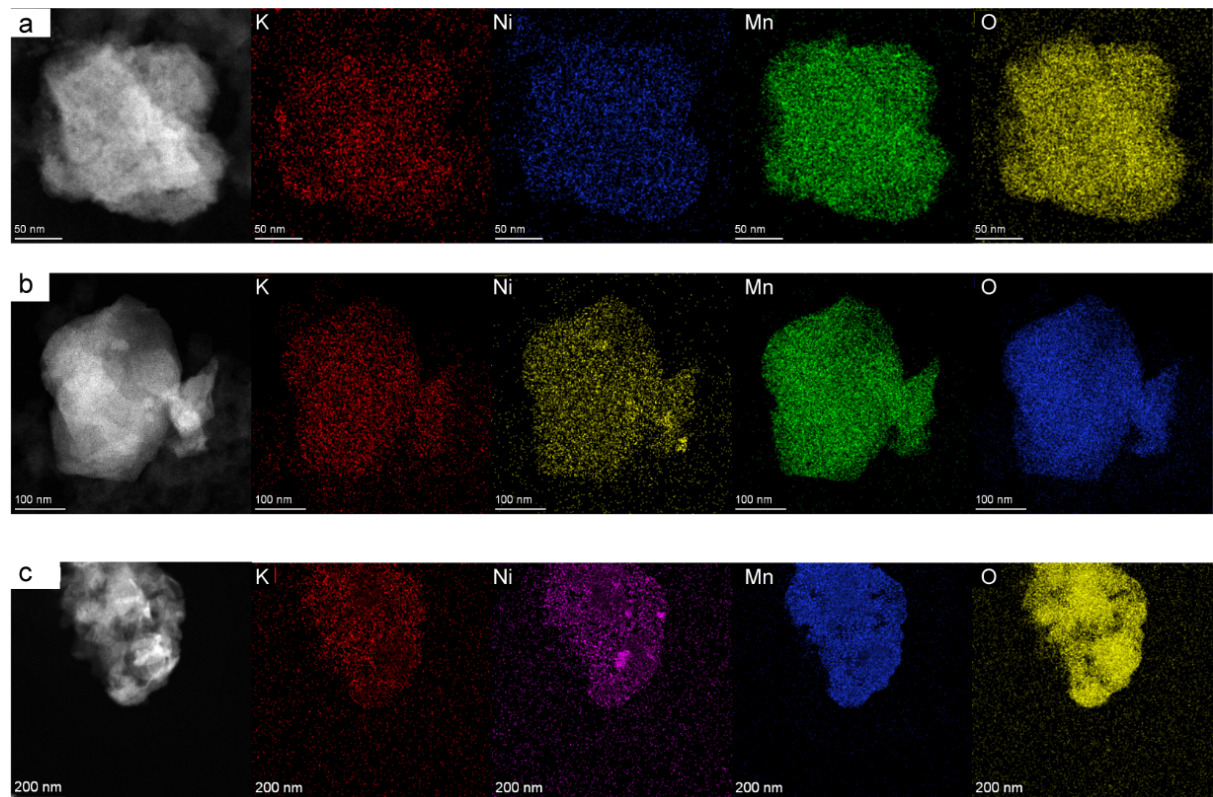


**Figure S15.** High-angle annular dark-field image (HAADF) image and EDS elecmmental mapping of P3-type  $K_{0.5}Ni_{1/3}Mn_{2/3}O_2$  particle at different state of (de)potassiation. (a) charge-4.2 V, (b) discharge-2.0 V, (c) discharge-1.5 V. We observed uniform elemental distributions in all cases.

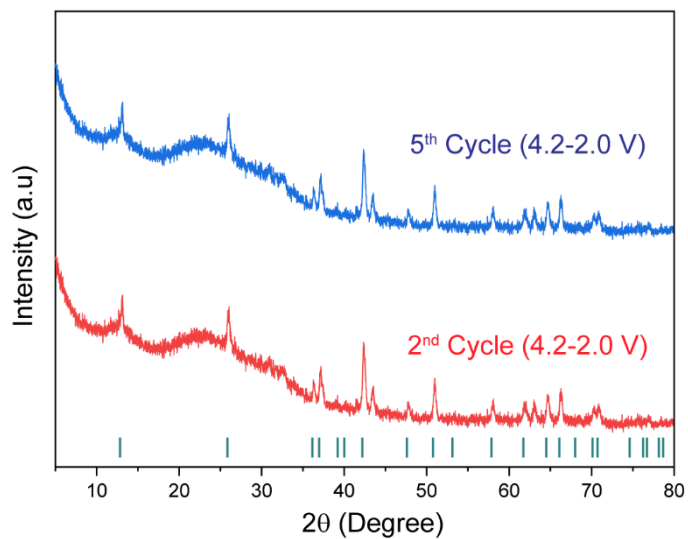


**Figure S16.** Ex-situ XRD ( $\lambda=1.5405\text{ \AA}$ ) at the end of 2<sup>nd</sup> and 5<sup>th</sup> cycle in the voltage window of 4.2-2.0 V.

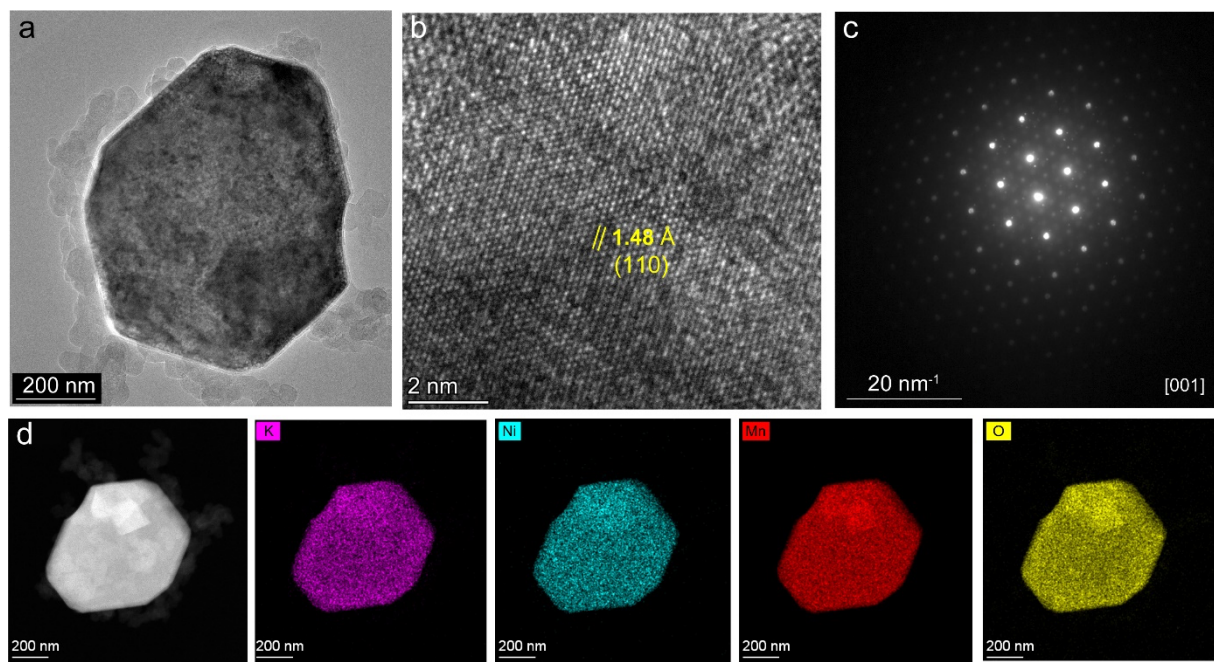


**Figure S17.** TEM analysis after 5<sup>th</sup> battery cycle in the potential window of 4.2-2.0 V. (a) bright field TEM micrograph, (b) HRTEM image showing lattice fringes corresponding to (110) planes. (c) SAED pattern showing intact superlattice spots along with regular spot with cycling, (d)) elemental mapping (TEM-EDS) confirming homogeneous distribution of K, Ni, Mn, and O elements.

**Table S5.** X-ray photoelectron spectroscopy (XPS) analysis of P3-type  $K_{0.5}Ni_{1/3}Mn_{2/3}O_2$  at different states of (de)potasssiation.

Mn		Pristine	Charge-4.2V	Discharge-2.0V	Discharge-1.5V
Mn- $2p_{3/2}$ (FWHM-1.2 eV)	4+	641.05	640.94	--	--
		642.12	641.85		
		642.28	642.89		
		643.90	643.95		
		646.26	645.27		
Mn- $2p_{3/2}$ (FWHM-1.1 eV)	3+	640.03	--	641.25	--
		641.36		642.00	
		641.49		643.05	
		642.99		644.21	
		645.07		645.34	
Mn $2p_{3/2}$ (FWHM-0.9 eV)	2+	--	--	--	641.01
					641.79
					642.59
					643.42
					644.57

Ni		Pristine	Charge-4.2V	Discharge-2.0V	Discharge-1.5V
Ni- $2p_{3/2}$	4+	--	858.96	--	--
Ni- $2p_{3/2}$	3+	855.95	854.71	858.64	858.95
Ni- $2p_{3/2}$	2+	854.15	--	853.88	854.06